Cellular/Molecular

Interneurons Produced in Adulthood Are Required for the Normal Functioning of the Olfactory Bulb Network and for the Execution of Selected Olfactory Behaviors

Vincent Breton-Provencher,[1] Morgane Lemasson,[1] Modesto R. Peralta III,[1] and Armen Saghatelyan[1,2]

[1]Cellular Neurobiology Unit, Centre de Recherche Université Laval Robert-Giffard, Québec, Québec G1J 2G3, Canada, and [2]Departement of Psychiatry, Université Laval, Québec, Québec G1K 7P4, Canada

Olfactory bulb (OB) interneurons are continuously renewed throughout an animal's lifespan. Despite extensive investigation of this phenomenon, little is known about bulbar circuitry functioning and olfactory performances under conditions of ablated arrival of new neurons into the adult OB. To address this issue we performed morphological, electrophysiological, and behavioral analysis in mice with suppressed bulbar neurogenesis. Infusion of the antimitotic drug AraC to the lateral ventricle via 28 d osmotic minipumps abolished the arrival of newly born neurons into the adult OB without affecting the total number of granule cells. The number, dendritic arborization, and spine density of interneurons generated in adulthood, before pump installation, were also not affected by AraC treatment. As a result of ablated neurogenesis, mitral cells—the principal output neurons in the OB—receive fewer inhibitory synapses, display reduced frequency of spontaneous IPSCs, experience smaller dendrodendritic inhibition, and exhibit decreased synchronized activity. Consequently, short-term olfactory memory was drastically reduced in AraC-treated mice. In contrast, olfactory performances of AraC-treated animals were undistinguishable from those of control mice in other odor-associated tests, such as spontaneous odor discrimination and long-term odor-associative memory tasks. Altogether, our data highlight the importance of adult neurogenesis for the proper functioning of the OB network and imply that new bulbar interneurons are involved in some, but not all, odor-associated tasks.

Introduction

In the adult brain, neuronal precursors born in the subventricular zone (SVZ) migrate toward the olfactory bulb (OB), in which they differentiate into granule and periglomerular neurons (Lledo and Saghatelyan, 2005), establish dendrodendritic synapses with the OB principal cells (Whitman and Greer, 2007), display appropriate electrophysiological features (Belluzzi et al., 2003; Carleton et al., 2003), and respond to odor stimulations (Carlén et al., 2002; Magavi et al., 2005). Interneurons generated in adulthood replace older granule cells and thus maintain the structural integrity of the OB network (Lagace et al., 2007; Ninkovic et al., 2007). The genetic ablation of adult neurogenesis led to the gradual decrease in the overall number of bulbar granule cells (Imayoshi et al., 2008). Surprisingly, however, even 6 months after ablation of bulbar neurogenesis the mice exhibited normal acquisition and retention of long-term odor-associated memory and unaltered odor discrimination (Imayoshi et al., 2008). In contrast, previous studies have demonstrated that mice with diminished OB neurogenesis displayed deficits in the odor discrimination tasks (Gheusi et al., 2000; Enwere et al., 2004) and that olfactory discrimination learning paradigm augmented the number of newborn interneurons in the odor-activated regions (Alonso et al., 2006; Mandairon et al., 2006). Moreover, odor enrichment, pheromones, and pregnancy increase the number of new bulbar interneurons, which is associated with an improved short-term odor memory, mating, and maternal behaviors (Rochefort et al., 2002; Shingo et al., 2003; Mak et al., 2007). Why diverse modulations in the level of adult neurogenesis give rise to different behavioral outcomes is currently unclear. It is noteworthy, however, that behavioral paradigms used in these studies are quite distinct and newborn neurons in the OB might be involved in some but not all odor-associated behavior. This hypothesis would be consistent with morphological and electrophysiological data showing distinct properties of OB interneurons born during the early postnatal period and in adulthood (Lemasson et al., 2005; Magavi et al., 2005; Saghatelyan et al., 2005). Thus, to understand the functional significance of adult neurogenesis, it is important to elucidate what are the exact morphological and electrophysiological alterations in the bulbar network following suppression of adult neurogenesis and then to test these animals in diverse odor-associated behavioral tasks.

To assess the role of newborn interneurons in the OB circuitry and their implication in the different odor-mediated tasks, we designed a series of morphological, electrophysiological, and behavior experiments to characterize the function of the bulbar network and the olfactory performances in mice with ablated

Received July 25, 2009; revised Sept. 24, 2009; accepted Oct. 26, 2009.

This work was supported by Canada Foundation for Innovation, Canadian Institutes of Health Research, and National Science and Engineering Research Council of Canada grants to A.S. A.S. is a recipient of the Canada Research Chair in Postnatal Neurogenesis. We thank Drs. Matthieu Guitton and Martin Beaulieu for advice on behavioral tests and members of the Saghatelyan lab for helpful discussions.

Correspondence should be addressed to Armen Saghatelyan, Centre de Recherche Université Laval Robert-Giffard, Université Laval, 2601 chemin de la Canardiere, Québec, QC G1J 2G3, Canada. E-mail: armen.saghatelyan@crulrg.ulaval.ca.

DOI:10.1523/JNEUROSCI.3606-09.2009

 0270-6474/09/2915245-13$15.00/0

adult neurogenesis. The proliferation of neuronal precursors in the SVZ was stopped via a 28 d osmotic minipump infusion of the antimitotic drug AraC into the lateral ventricle. Using electrophysiological recordings, we show for the first time the changes on cellular and network levels in the bulbar circuitry lacking new neurons. Suppressing the arrival of new neurons to the OB reduces the mitral cell inhibition and alters their synchronized activity. Consequently, mice with ablated neurogenesis display alterations in some, but not all, odor-associated behavior. Together, our data provide new functional insights into the role of new neurons in the OB.

Materials and Methods

Animals

All experiments were performed in adult two- to three-month-old C57BL/6J male mice (Charles River) in accordance with Laval University guidelines. Osmotic minipumps (Alzet Osmotic Pump, model 1004) were filled either with saline (NaCl 0.9%) or antimitotic drug AraC (2.0% in saline) and implanted into the lateral ventricle of one hemisphere using the following coordinates (with respect to the bregma): anterior–posterior, 0.40 mm; medial–lateral, 0.90 mm; and dorsal–ventral, 2.15 mm. After pump installation, all mice were housed individually. All the following experiments were performed with the experimenter being "blind" to the treatment. After every experiment, the level of doublecortin (Dcx) in the olfactory bulb (OB) was verified and results from animals showing <70–80% reduction of Dcx were discarded. Similar reduction in Dcx expression was observed in both ipsilateral and contralateral OB.

Stereotaxic injection

GFP-encoded lentivirus was stereotaxically injected into the rostral migratory stream of both hemispheres of the adult mouse brain 28 d before the pump installation. The following coordinates were used (with respect to bregma): anterior–posterior, 2.55 mm; medial–lateral, 0.82 mm; and dorsal–ventral, 3.15 mm. The morphology and spine density of the cells generated before the ablation of neurogenesis were assessed after the control and AraC treatment (28 d infusion period).

Western blot analysis

Twenty-eight days after NaCl or AraC infusion, the OBs were extracted and homogenized in lysis buffer (50 mM HCl, pH 7.5, 1 mM EDTA, 1 mM EGTA, 1 mM sodium orthovanadate, 50 mM sodium fluoride, 5 mM sodium pyrophosphate, 10 mM sodium β-glycerophosphate, 0.1% 2-mercaptoethanol and 1% Triton X-100) containing Protease Inhibitor Cocktail Set III (Calbiochem). The homogenates were sonicated and centrifuged at 13,000 × *g* at 4°C for 20 min to remove insoluble fraction. Protein samples (70 μg) were separated on a NuPage 4–12% Bis-Tris gel (Invitrogen) and transferred to nitrocellulose membranes (GE Healthcare Bioscience). Dcx- and actin-immunoreactive bands were detected using rabbit polyclonal IgG (1:1000; US Biological) and mouse monoclonal IgG (1:2000; Sigma) antibodies, respectively. Secondary antibody (goat anti-rabbit HRP 1:5000, Millipore Bioscience Research Reagents; and goat anti-mouse HRP 1:1000, Bio-Rad) and a chemiluminescence substrate mixture (ECL, GE Healthcare) were then used to detect the bands. The expression levels of Dcx in AraC and NaCl mice were normalized to the level of actin.

Patch-clamp recordings

Twenty-five to twenty-eight days after the placement of the pumps, deeply anesthetized animals were transcardially perfused with modified oxygenated artificial CSF (ACSF) containing the following (in mM): 250 sucrose, 3 KCl, 0.5 $CaCl_2$, 3 $MgCl_2$, 25 $NaHCO_3$, 1.25 $NaHPO_4$, and 10 glucose. OBs were then quickly removed and placed into normal oxygenated ACSF containing the following (in mM): 124 NaCl, 3 KCl, 2 $CaCl_2$, 1.3 $MgCl_2$, 25 $NaHCO_3$, 1.25 $NaHPO_4$, and 10 glucose. Horizontal slices (250 μm thick) were obtained using a vibratome (VT1000S, Leica). During electrophysiological experiments, slices were superfused with oxygenated ACSF at a rate of 2 ml/min. Recordings were performed with the Multiclamp 700B amplifier (Molecular Devices). Patch electrodes (ranging from 2.5 to 4 MΩ) were filled with an intracellular solution, which for all experiments (except the measurement of potassium currents) contained the following (in mM): 135 CsCl, 10 HEPES, 0.2 EGTA, 2 ATP, 0.3 GTP, and 10 glucose. After every experiment, slices were fixed with 4% paraformaldehyde. Dcx expression was then verified by performing immunohistochemistry on each slice with methanol and acetone pretreatment to improve permeabilization.

In some electrophysiological recordings, 5.4 mM biocytin was added to the intracellular solution to reveal the morphology of the recorded cells via immunohistochemistry with a rhodamine(tetramethylrhodamine isothiocyanate) [rhodamine(TRITC)]-conjugated streptavidin antibody (Jackson ImmunoResearch). Spontaneous inhibitory currents (sIPSCs) were isolated by the bath application of kynurenic acid (Kyn, 5 mM) to block glutamatergic activity. Miniature IPSCs (mIPSCs) were isolated by the application of tetrodotoxin (TTX, 1 μM) in the presence of Kyn to block voltage-dependent sodium channels. Synaptic responses were analyzed with the MiniAnalysis program (Synaptosoft). Evoked dendrodendritic currents were recorded in Mg^{2+}-free ACSF containing 1 μM TTX to block Na^+ channel activity. We used a $GABA_A$ receptor antagonist, (−)-bicuculline methochloride (BMI; 50 μM) to isolate evoked dendrodendritic inhibitory (DDI) responses. The traces representing DDI were obtained by subtracting the currents recorded under control conditions (Mg^{2+}-free ACSF containing 1 μM TTX) from those recorded in the presence of BMI. The amplitude and the charge of the DDI were normalized to the recorded cell capacitance.

Sodium and potassium activation and deactivation curves were examined using a voltage step protocol ranging from −100 to 30 mV. Sodium currents were isolated by subtracting the traces obtained with and without the application of TTX. For potassium currents, CsCl was replaced by 135 mM K-gluconate in the intracellular solution. The two different currents were isolated by the subsequent bath application of 5 mM 4-aminopyridine (4AP) and 9 mM tetraethylammonium chloride (TEA).

Local field potential recordings

For the recording of local field potentials (LFPs), pipettes were filled with 2 M NaCl and the slices (same preparation protocol as in patch-clamp recordings) were maintained at 35°C throughout the recording. The olfactory nerve was stimulated (stimulation strength: 150–250 μA) using an A360 stimulus isolator (World Precision Instruments). We recorded with multiclamp 700B amplifier (Molecular Devices) the oscillations close to the mitral cell layer in normal ACSF and with a $GABA_A$ receptor antagonist, gabazine (20 μM). Only the recordings showing a significant reduction of the oscillation index in the presence of gabazine were kept for analysis. For analysis of LFP oscillation, we used a customized program written in Matlab (The Matworks) to calculate the frequency spectrum and the autocorrelation trace of the signal using a fast-Fourier transform algorithm. The oscillation index, a measurement of the oscillation power, was calculated as follows:

$$\text{Oscillation index} = \frac{\int_{20}^{80} \text{DFT}_{\text{pre}}(f)df}{\int_{20}^{80} \text{DFT}_{\text{post}}(f)df},$$

where $\text{DFT}_{\text{pre}}(f)$ and $\text{DFT}_{\text{post}}(f)$ represent a discrete Fourier transform evaluated on a 200 ms time window taken before and after the stimulus, respectively. This formula represents a sum of the oscillation amplitudes at all frequencies between 20 and 80 Hz after the stimulus normalized to the frequency amplitudes (from the same range) taken before the stimulus. Note that similar results were obtained when oscillation index was defined as the second peak height of the normalized autocorrelation function.

Immunohistochemistry and BrdU labeling

Immunohistochemistry and BrdU labeling were performed as described previously (Snapyan et al., 2009). Briefly, the DNA synthesis marker 5-bromo-2′-deoxyuridine (BrdU; Sigma) was dissolved in a sterile solution of 0.9% NaCl and 1.75% NaOH (0.4 N). This solution was injected

intraperitoneally at a concentration of 50 mg/kg body weight. Four injections of BrdU spaced 2 h apart were administrated 21 d before pump installation. Coronal sections of the OB and dentate gyrus (DG) were immunostained with the primary antibody raised against Dcx (goat polyclonal IgG 1:1000; Santa Cruz Biotechnology), NeuN (mouse monoclonal IgG 1:200; Millipore Bioscience Research Reagents), and BrdU (rat polyclonal IgG 1:500; Serotec). The secondary antibodies used were donkey anti-goat IgG and goat anti-mouse IgG (Invitrogen) and biotinylated goat anti-rat IgG (Thermo Scientific). BrdU immunostaining was revealed with diaminobenzidine (0.05%), to which 0.005% H_2O_2 was added. Sections were analyzed using either a standard microscope equipped with a motorized stage (BX51; Olympus) for Dcx and BrdU staining or with an FV1000 confocal microscope equipped with Ar 488, HeNe1 543, and HeNe2 633 lasers (Olympus). The density of Dcx^+ cells in the DG was obtained by normalizing the number of immunopositive cells to the length of the DG. For NeuN quantification, a single optical image was taken in the different regions of the OB (medial, ventral, lateral, and dorsal) with a 40× objective. The number of $NeuN^+$ cells was counted over the area of these images. For BrdU quantification, the number of BrdU cells was counted manually over the whole area of the granule cell layer. Dcx^+, $NeuN^+$, and $BrdU^+$ cells were quantified in each third serially cut 40-μm-thick section. Immunostainings for Dcx, NeuN, and BrdU were performed 28 d after infusion of NaCl or AraC.

Immunostaining for gephyrin, a scaffolding protein for postsynaptic $GABA_A$ receptors, was performed 25–28 d after NaCl or AraC infusions. We used a mouse monoclonal IgG antibody against gephyrin (1:1000, Synaptic Systems), on the slice having mitral cells filled with biocytin during electrophysiological recording. Biocytin staining was revealed with rhodamine (TRITC)-conjugated streptavidin antibody. Gephyrin immunostaining was revealed with goat anti-mouse IgG 488 secondary antibody (Invitrogen). For each mitral cell, 10 randomly chosen areas of interest on the lateral dendrites were imaged with a 100× objective. Counting of the number of gephyrin puncta located on the lateral dendrites of the mitral cell was done along the entire z axis (z resolution is 0.46 μm) and data are presented as the number of gephyrin puncta over the dendritic volume. To obtain the average value of gephyrin puncta for each mitral cell, we averaged the data gathered from 10 images. These data were then averaged across the cells to obtain the mean values for control and AraC-treated animals.

Behavior

Locomotion. Five days after pump installation until the end of the experiment, mice were kept in a reversed 12 h light/dark cycle with illumination started at 8:00 P.M. The animals had access to water and food *ad libitum*. Twenty-eight days after osmotic pump installation, the motility of the NaCl- or AraC-treated mice was tested using the VersaMax animal activity monitoring system (AccuScan Instruments). The testing chamber represents an 18 × 18 × 18 cm transparent enclosure equipped with three rows of photocells sensitive to infrared for movement detection. The mouse was placed in the detection chamber for an hour and its spontaneous locomotion was analyzed automatically by the VersaMax software.

Object recognition. The object recognition task to evaluate the recognition memory was performed as described previously (Bevins and Besheer, 2006). The animals were kept on a reverse light/dark cycle starting from the fifth day after pump installation. After being habituated for 2 d (26–27 d after pump installation) to the testing chamber (Plexiglas enclosure; dimensions, 21 × 25 × 46 cm), mice were familiarized with the first object (object A). For this familiarization phase, two identical objects (object A) were placed on both sides of the cage. Animals were individually allowed, from the middle of the cage, to freely explore the two objects for a period of 10 min. Then, they were returned to their home cage. One hour later, recognition of the object A was tested during a 5 min period. For this, two different objects were presented: the familiar object (object A) and a novel object (object B). The time exploring both objects was recorded during the two phases of the object recognition test. We considered the animal to be exploring when its mouth, nose, or paws were in direct contact with the object. The test chamber was washed at the end of each trial.

Novelty suppressed feeding behavior. Spontaneous motivation was assessed using the novelty suppressed feeding behavior test (Britton and Britton, 1981). Animals for this test were kept in a normal light/dark cycle but were food deprived 3 d after the pump installation. Each animal was weighed daily and fed with sufficient diet D10001 (Research Diets) to maintain 80–85% of their free feeding weight. Water was available *ad libitum*. Starting from the 27th day after pump installation, the animals were habituated for 2 d to the Plexiglas testing chamber (21 × 25 × 46 cm). For the test performed at the 29th day after pump installation, a dish containing food pellet (Froot Loops, Kellogg's) was placed on one end of the Plexiglas chamber and food-deprived mice were individually and gently placed on the opposite end. The latency to start consumption of the Froot Loops was recorded. The cage was properly cleaned after each animal.

Tail suspension. Mice were tested for anxiety with the tail suspension test (Crowley et al., 2004). We performed this behavioral paradigm at the 25th day after osmotic pump installation and on the same group of animals tested in novelty-suppressed feeding behavior. The tail suspension apparatus (Med-Associates) consisted of a box (32 × 33 × 33 cm) with an aluminum bar used to suspend the mouse by the tail. We calculated the total duration of immobility of animals over the 6 min period as a measure of anxiety.

Odor detection threshold. After a 4 d habituation to the experimental procedures, we evaluated the odor detection threshold of the AraC- and NaCl-treated mice at the 26th to 28th day after the osmotic pump installation. The animals were kept on reverse light/dark cycle (same protocol as for the locomotion paradigm). The animals' home cage was used as the testing chamber, albeit with a clean unused cover grid to hang pipettes containing the odors. The same procedure was also used for the odor discrimination and the short-term odor memory paradigms. During a 5 min period, each animal was exposed to two Pasteur pipettes containing saturated filter paper, one a control (mineral oil) and the other odorized with different concentrations of octanol or isoamyl acetate or limonene-(−). Sniffing time was measured for four concentrations (10^{-7}, 10^{-5}, 10^{-4}, and 10^{-3}%) tested in separate sessions, in an ascending order. The animals were considered to be able to detect olfactory stimulus when they spent more time investigating the odor than the mineral oil.

Odor discrimination. The olfactory discrimination task is a habituation–dishabituation test. Reverse light/dark cycle mice, previously habituated to experimental procedures, were familiarized with a first odor (odor of habituation) in four successive sessions and then exposed once to a novel odor (odor of dishabituation). The duration of each session was 5 min and they were separated by 15 min intervals. Discrimination abilities of the mouse were analyzed using two different groups of odors, tested randomly in separate sessions: butyraldehyde and isoamyl acetate; 2-heptanol and limonene-(−) (each from Sigma-Aldrich). The concentration of each odor used was 10^{-3}. We considered that mice were able to discriminate a novel odor from a familiar one when the time of exploration in the dishabituation session was greater than the time of exploration observed in the fourth habituation session.

Long-term odor-associative memory. This olfactory learning and memory test was conducted in two phases exactly as described by Imayoshi et al. (2008). During a 4 d training phase, food-restricted animals (see protocol for novelty-suppressed feeding behavior) received four 10 min trials: two trials in which one odor [carvone-(+): 6.4 M] was presented in association with a sugar reward and two other trials in which a different odor [carvone-(−): 6.4 M] was presented without the sugar. Twelve hours or 7 d after training (21st and 28th days after osmotic minipump installation, respectively), we tested the ability of mice to memorize the association of one odor to a reward and another odor with no reward. Animals were exposed to the two odors placed in two separated cups under 5 cm of Pro Chip bedding without reward. The time the mouse spent digging the bedding in each cup containing odor was recorded during a 2 min period. This test was conducted in a large Plexiglas enclosure (21 × 25 × 46 cm).

Olfactory short-term memory. After a 4 d habituation, reverse light/dark cycle mice (see protocol for locomotion) were exposed to the same odor during two different 5 min sessions separated by 30, 60, 90, and 120 min intervals. These tests were performed from the 26th to the 28th day

after osmotic minipump installation. The pipette containing the odor was inserted randomly in the cage grid to avoid a spatial recognition effect. The following odors were used: (+) terpinen-4-ol, limonene (−), isoamyl acetate, and octanol. Each time period and odors (all at a concentration of 10^{-3}) were tested randomly between the animals. A significant decrease in the time of exploration on the second odor exposure was considered as an indication that the animal remembered the odor.

Statistical analysis

Data are presented as mean ± SEM. Statistical significance was tested by using Student's *t* test (with $^{*}p < 0.05$ and $^{**}p < 0.01$).

Results

Treatment with an antimitotic drug abolished the arrival of new neurons in the OB

To assess the functional role of neurogenesis in the OB we ablated the arrival of new neurons via infusion of the antimitotic drug AraC into the lateral ventricle for a 28 d period. AraC infusion did not affect the overall health of the animals, as attested by the fact that mice continued to gain weight normally (data not shown). Immunostaining for Dcx, a marker for migrating neuroblasts, revealed numerous Dcx^+ cells in the OB of saline-treated control animals, but not in AraC-infused mice (Fig. 1*A*). Quantitative Western blot analysis of Dcx expression in the OB revealed a 75.3 ± 9.4% ($n = 4$ animals for both conditions) reduction in the AraC-treated animals compared with the controls (Fig. 1*B*). Interestingly, AraC infusion into the lateral ventricle was less efficient on DG neurogenesis. While in the OB Dcx immunostaining was practically absent (Fig. 1*A*), only a twofold reduction in the density of Dcx^+ cells in the subgranular layer of DG was observed (0.024 ± 0.002 for control; $n = 4$ animals and 0.010 ± 0.001 for AraC-treated; $n = 7$ animals; $p < 0.001$) (Fig. 1*C*). Therefore, infusion of an antimitotic drug to the lateral ventricle suppress substantially the arrival of new bulbar neurons and may, thus, serve as a good model for the assessment of the functional importance of adult OB neurogenesis.

Ablation of OB neurogenesis does not affect the pre-existing population of interneurons

Interneuronal precursors that are continuously sent to the OB differentiate mostly into granule cells (Hack et al., 2005; Lagace et al., 2007; Ninkovic et al., 2007) and are required for the structural maintenance of the bulbar network (Imayoshi et al., 2008). Genetic ablation of adult neurogenesis for >6 weeks, but not 21 d, induces a decrease in the overall number of granule cells (Imayoshi et al., 2008). In agreement with this, our immunohistochemical analysis of neuronal marker $NeuN^+$ cells in the dorsal, lateral, medial, and ventral parts of the granule cell layer of the OB, 28 d following pharmacological ablation of adult neurogenesis, did not reveal any significant difference between control and AraC-treated animals ($n = 4$ animals per group) (Fig. 2*A*,*B*). To investigate how ablation of neurogenesis affects the subpopulation of pre-existing granule cells generated in adulthood, we injected 5-bromo-2′-deoxyuridine (BrdU) 21 d before osmotic minipumps installation. The number of cells generated 3 weeks before suppression of neurogenesis for 28 d was not changed as demonstrated by the quantification of the BrdU labeled profiles in the granule cell layer (375 ± 44 and 327 ± 16 $BrdU^+$ cells per mm^2 for NaCl- and AraC-treated mice, respectively; $n = 4$ animals for each condition). Even though the density of the granule cells generated before the suppression of neurogenesis remained unchanged, it is possible that a continuous supply of interneurons is required for preserving the normal dendritic morphology and spine density of pre-existing granule cells. To explore this possibility we labeled the newly born granule cells via a stereotaxic injection of GFP lentivirus into the rostral migratory stream 28 d before the osmotic minipumps installation. GFP^+ granule cells were widely distributed in the control and AraC-treated animals and displayed normal morphology (Fig. 2*C*). Indeed, the length of primary (101 ± 9 μm; $n = 31$ cells and 97 ± 8 μm; $n =$

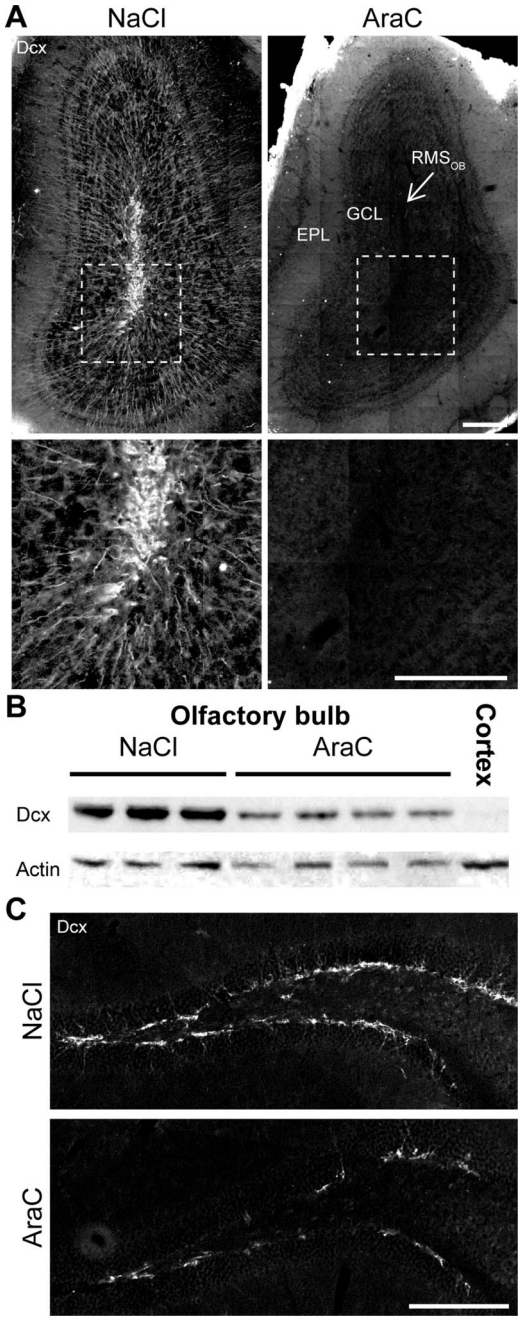

Figure 1. Infusion of antimitotic drug, AraC, abolishes neurogenesis in the adult olfactory bulb but not in the hippocampus. ***A***, Top, Immunostaining for Dcx in coronal sections of the OB of control (NaCl) and AraC-treated animals. Note the absence of immunofluorescence in the rostral migratory stream of the OB (RMS_{OB}) and the granular cell layer (GCL) in the AraC-treated mouse. EPL, External plexiform layer. Bottom, Enlarged view of boxed regions. ***B***, Western blot analysis of OBs samples showing a drastic reduction of Dcx following a 28 d AraC infusion into the lateral ventricle. A cortical sample was used as a control, to assure Dcx antibody specificity. ***C***, Dcx immunostaining in hippocampal coronal sections of NaCl- and AraC-treated animals. Note that AraC infusion into the lateral ventricle affects neurogenesis in the dentate gyrus to a lesser degree compared with the OB. Scale bars, 200 μm.

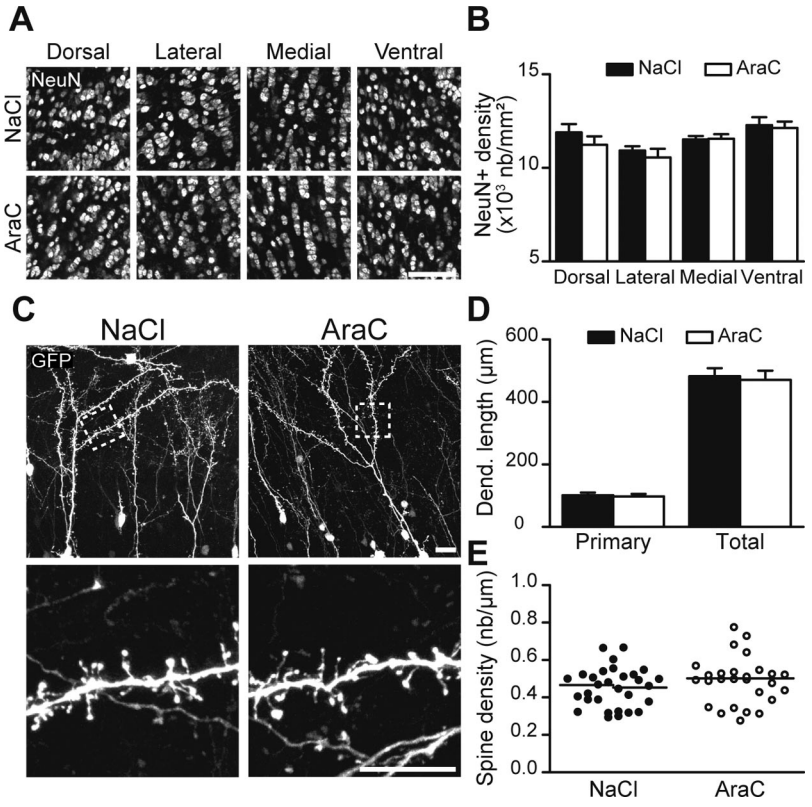

Figure 2. The pre-existing population of interneurons is unaffected by the AraC treatment. ***A***, Immunostaining for the neuronal marker NeuN in the different regions of the OB derived from control (NaCl) and AraC-treated animals. Scale bar, 50 μm. ***B***, NeuN $^+$ cell density quantification in the dorsal, lateral, medial, and ventral OB regions. Data are presented as mean $\pm$ SEM ($n = 4$ animals per group). ***C***, Top, Confocal images of GFP $^+$ granule cells revealing their complete morphology. These cells were labeled with an injection of GFP-encoding lentivirus in the rostral migratory stream 28 d before the NaCl or AraC treatment. Bottom, Higher magnification of boxed regions showing the spine density of the adult-generated granule cells. Scale bars, 20 μm. ***D***, No changes in the primary dendrite length (calculated as the length of the dendrite from the soma to the first point of ramification) or the total dendritic length (excluding the primary dendrite) were observed in GFP $^+$ cells between the control and neurogenesis-ablated OBs. Data are presented as mean $\pm$ SEM ($n = 31$ and 27 cells for control and AraC-treated groups, respectively). ***E***, Spine density quantification of GFP $^+$ cells generated in adulthood. Each point represents the spine density of individual cell, whereas horizontal bars represent the mean values for NaCl and AraC treatments.

27 cells for 28-d-treated NaCl and AraC mice, respectively) or secondary dendrites (482 $\pm$ 26 μm; $n = 31$ and 470 $\pm$ 30 μm; $n = 27$ cells for NaCl- and AraC-treated mice, respectively) was not affected (Fig. 2*D*). Moreover, stopping neurogenesis for 28 d does not impinge on the spine formations of adult-generated cells already in place. Their spine density remains stable after the AraC treatment (0.45 $\pm$ 0.02 spines/μm; $n = 30$ for control and 0.49 $\pm$ 0.02 spines/μm $n = 27$ cells for neurogenesis deprived animals) (Fig. 2*C*,*E*). Thus, the constant arrival of new neurons is not required for the maintenance of the number, dendritic morphology and spine density of the pre-existing granule cells generated during adulthood.

Suppression of OB neurogenesis alters IPSCs received by the mitral cells

The granule cells, which are constantly replaced by adult olfactory neurogenesis, form synaptic connections on mitral cells, the principal neurons in the bulbar circuitry. The dendrodendritic reciprocal synapses formed by these neurons, consist of an excitatory mitral-to-granule cell synapse directly adjacent to an inhibitory granule-to-mitral cell synapse (Price and Powell, 1970; Whitman and Greer, 2007). Therefore, the sources of inhibitory inputs received by mitral cells might be subdivided in three groups: (1) glutamate-induced GABA release [spontaneous postsynaptic currents (sPSCs)], (2) the action potential-dependent GABA release (sIPSCs), and (3) the inhibitory currents independent of both glutamate receptor activation and action potentials, herein called mIPSCs. To understand on a cellular level the functional consequences of an impaired neurogenesis, we performed patch-clamp recordings from mitral cells. We first recorded sPSCs from those neurons (Fig. 3*A*, upper traces) in the normal and neurogenesis-deficient OB slices, then sIPSCs by blocking glutamatergic receptors with kynurenate (Kyn, 5 mM) (Fig. 3*A*, middle traces) and finally mIPSCs by blocking voltage-dependent Na^+ channels with TTX (1 μM) in the presence of Kyn (Fig. 3*A*, lower traces). Interestingly, the frequency of sPSCs (47.0 $\pm$ 3.4 Hz for control; $n = 9$ cells and 28.4 $\pm$ 3.9 Hz for AraC-treated; $n = 8$ cells; $p < 0.01$); sIPSCs (14.3 $\pm$ 1.7 Hz for NaCl; $n = 9$ cells and 6.9 $\pm$ 0.9 Hz for AraC-infused; $n = 8$; $p < 0.01$) and mIPSCs (5.3 $\pm$ 1.0 Hz for control; $n = 9$ cells and 2.9 $\pm$ 0.3 Hz for AraC-treated; $n = 8$ cells; $p < 0.05$) were reduced following the ablation of neurogenesis (Fig. 3*B*). In contrast, the amplitude of sPSCs (63.4 $\pm$ 3.3 pA for control; $n = 9$ cells and 61.7 $\pm$ 4.5 pA for AraC-treated mice; $n = 8$ cells); sIPSCs (49.3 $\pm$ 4.0 pA for control; $n = 9$ cells and 43.7 $\pm$ 5.6 pA for AraC-treated mice; $n = 8$ cells) and mIPSCs (31.9 $\pm$ 3.6 pA for control; $n = 9$ cells and 27.4 $\pm$ 3.4 pA for AraC-treated mice; $n = 8$ cells) were not affected (Fig. 3*C*). Moreover, the rise time (2.55 $\pm$ 0.12 ms for control and 2.57 $\pm$ 0.09 ms for AraC-treated; $n = 9$ and 8 cells, respectively) and decay time (16.6 $\pm$ 0.5 ms for NaCl- and 16.4 $\pm$ 0.8 ms for AraC-treated mice; $n = 9$ and 8 cells, respectively) of mIPSCs were not distorted by AraC infusion (Fig. 3*D*,*E*). To assess the possible alterations in the glutamate-induced and action-potential-dependent GABA release following suppression of neurogenesis we compared the percentage of reduction in the frequency and amplitude after applications of Kyn and TTX in the saline and AraC-infused animals. No changes in these parameters were observed (data not shown). Thus, while comparable amplitude and kinetics of mIPSCs are indicative for the normal content and functioning of postsynaptic $GABA_A$ receptors on the mitral cells, the changes in the frequency of miniatures are suggestive for the reduction in the number of GABAergic synapses in neurogenesis-deprived animals.

To analyze evoked granule-to-mitral cell responses in control and AraC-infused animals, we briefly depolarized mitral cells using a voltage step (50 ms and 60 mV) and recorded from same-cell DDI currents (Fig. 3*F*). The normalized amplitudes (60.9 $\pm$ 14.5 pA/pF for control; $n = 5$ cells and 29.6 $\pm$ 4.7 for AraC-treated; $n = 6$ cells; $p = 0.053$) as well as the normalized charges

(39.8 ± 7.1 pC/pF for control; $n = 5$ cells and 16.3 ± 4.7 pC/pF for AraC-treated; $n = 6$ cells; $p < 0.05$) of the DDI were smaller in the neurogenesis-deficient animals (Fig. 3*G*). Together, these experiments demonstrate the importance of a continuous neurogenesis for the maintenance of the normal inhibitory input onto the target cells in the OB.

Suppression of neurogenesis decreases the number of GABAergic synapses on the mitral cells

As stated above, the most plausible explanation for the decreased inhibition in the OB of AraC-treated animals is a reduction in the number of GABA release sites. Alternatively, the reduced spontaneous and evoked inhibitory activity recorded in neurogenesis-deprived OB principal neurons could arise from either changes in the morphology or membrane properties of mitral cells. We, therefore, examined the primary and secondary dendrite lengths of the biocytin-filled mitral cells used for electrophysiological recordings (Fig. 4*A*). The length of the primary (278 ± 26 μm for control; $n = 10$ cells and 287 ± 27 μm for AraC-treated; $n = 9$ cells) or secondary (1637 ± 98 μm for saline-treated; $n = 10$ cells and 1525 ± 132 μm for AraC-infused; $n = 9$ cells) dendrites was similar in the control and neurogenesis-deprived OB (Fig. 4*B*). No changes in the mitral cells passive membrane properties, such as resting membrane potential, capacitance, and membrane resistance, were observed (data not shown). In addition, spontaneous firing activity of mitral cells recorded in the cell-attached mode, in the presence of Kyn (5 mM) and BMI (50 μM) to block synaptic transmission, was undistinguishable between control and neurogenesis-deficient animals (3.5 ± 0.6 Hz for the control; $n = 9$ cells and 3.2 ± 1.1 Hz for AraC-treated; $n = 10$ cells). In agreement with these results, voltage-dependent Na^+ and K^+ currents recorded from the mitral cells in the OB of AraC-treated animals were similar to those obtained in the control animals. The TTX-sensitive Na^+ currents along with the 4AP- and TEA-sensitive K^+ current activation (Fig. 4*C–E*) and inactivation (data not shown) curves were identical with or without the ablation of neurogenesis ($n = 10$ cells in NaCl and 11 cells in AraC treatment for Na^+ currents; $n = 7$ cells in both treatments for K^+ currents). These experiments revealed that the changes in the inhibitory input seen in the mitral cells of AraC-treated animals do not result from a variation in the size or membrane properties of these principal neurons.

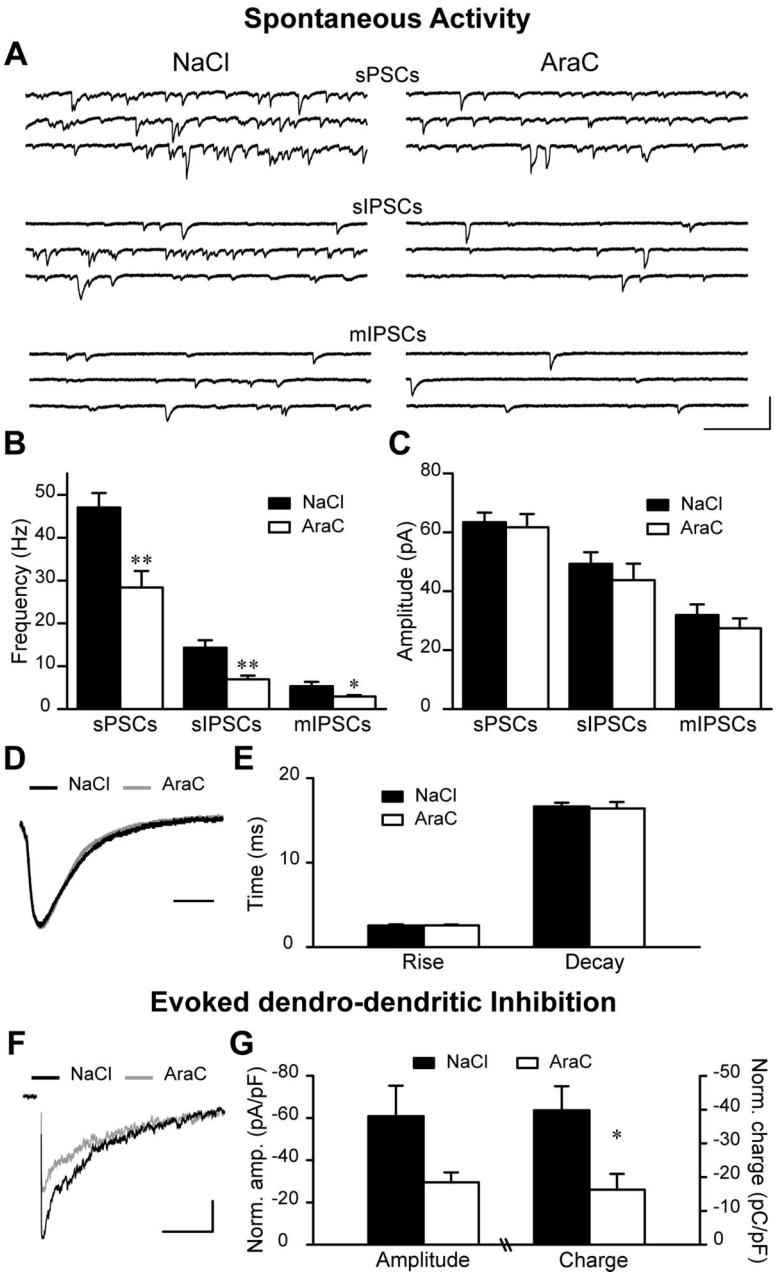

Figure 3. Suppression of OB neurogenesis reduces inhibition on mitral cells. ***A***, Individual experiments illustrating sPSCs, sIPSCs, and mIPSCs recorded from OB mitral cells of control (NaCl) and AraC-treated animals. Calibration: 100 ms, 500 pA. ***B***, ***C***, Quantification of the mean frequencies (***B***) and amplitudes (***C***) of sPSCs, sIPSCs, and mIPSCs. Data are presented as mean ± SEM ($n = 9$ and 8 cells for NaCl- and AraC-treated animals, respectively). *$p < 0.05$, **$p < 0.01$; Student's *t* test. ***D***, Average mIPSCs from two single cells. The amplitudes of traces taken from control (black trace) and AraC-treated (gray trace) recordings were scaled to highlight unaltered kinetics of mIPSCs. Calibration: 10 ms. ***E***, Quantification of mIPSCs decay and rise times. Data are presented as mean ± SEM ($n = 9$ and 8 cells for NaCl- and AraC-treated animals, respectively). ***F***, Traces illustrating the dendrodendritic inhibition (DDI) following a 50 ms depolarizing step in mitral cells recorded from NaCl (black trace) and AraC-treated (gray trace) mice. Calibration: 500 ms, 1 nA. ***G***, Quantification of the DDI amplitude (left) and charge (right) recorded from mitral cells in NaCl and AraC bulbs. The amplitude and charge of DDI were normalized (Norm. charge) to the capacitance for each recorded cell. Data are presented as mean ± SEM ($n = 5$ and 6 cells for control and AraC-infused animals, respectively). *$p < 0.05$; Student's *t* test.

Thus, all evidence points toward a reduction in the number of GABAergic synapses following the ablation of bulbar neurogenesis as a structural basis underlying the decrease in the inhibitory input onto the mitral cells. We, therefore, examined the number of postsynaptic GABAergic sites identified by gephyrin immunostaining on the lateral dendrites of the biocytin-filled mitral cells (Fig. 4*F*,*G*). Quantification of gephyrin$^+$ puncta per volume

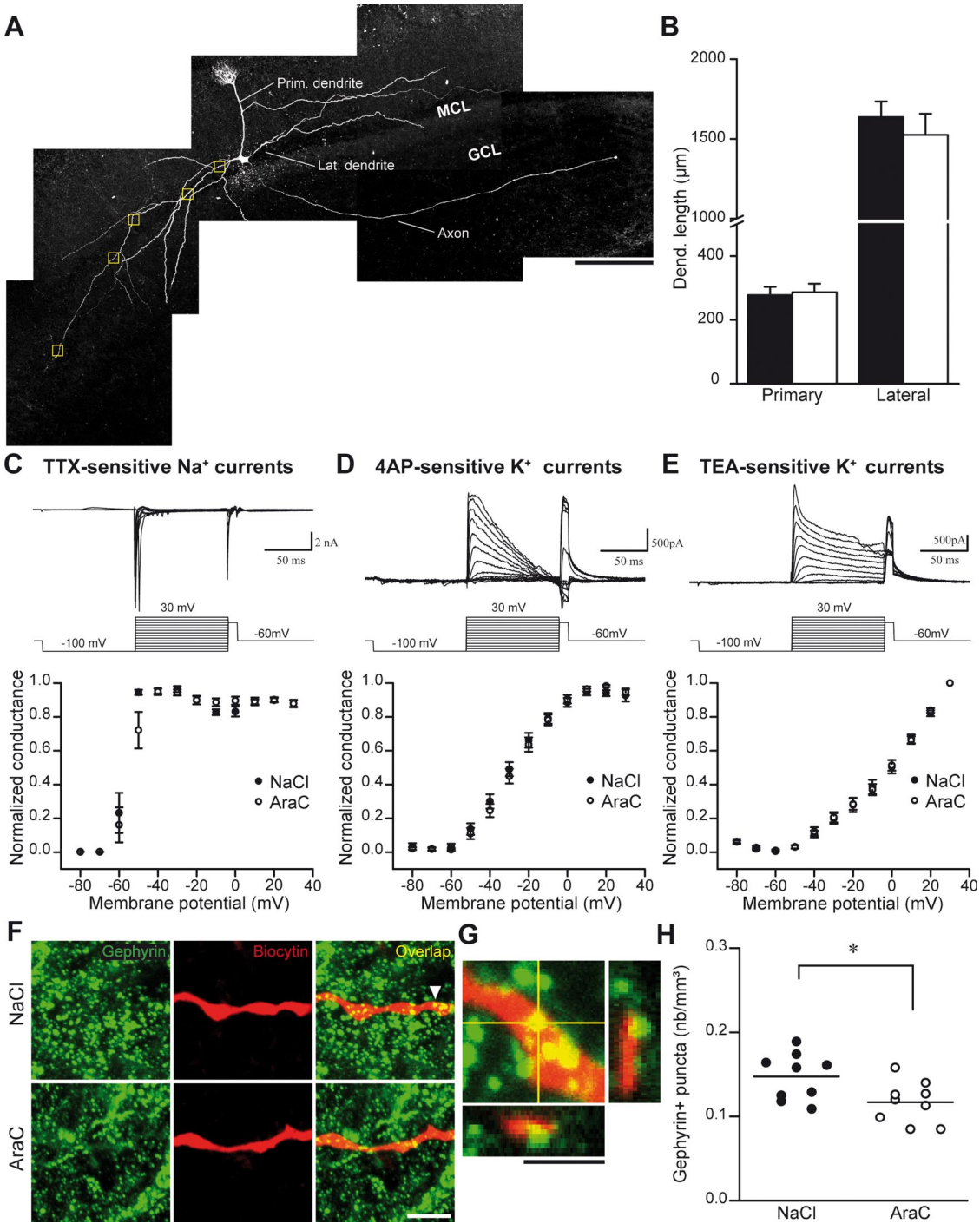

Figure 4. Reduced number of GABAergic postsynaptic sites on the mitral cells lateral dendrite after the suppression of neurogenesis. ***A***, Reconstitution of confocal images of the mitral cells filled with biocytin. MCL, Mitral cell layer; GCL, granule cell layer. The boxed regions show an example of sampling used for the quantification shown in ***H***. ***B***, Morphological analysis of the mitral cells demonstrating no significant difference in the primary and lateral dendrite lengths when neurogenesis is stopped. Data are presented as mean ± SEM ($n = 10$ and 9 cells for control and AraC-treated animals, respectively). ***C–E***, Membrane properties of mitral cells in control (NaCl) and AraC-treated animals. Top, Individual experiments illustrating TTX-sensitive Na^+ currents and TEA- and 4AP-sensitive K^+ currents recorded in mitral cells. Calibration: ***C***, 2 nA, 50 ms; ***D***, ***E***, 500 pA, 50 ms. Bottom, Plot of the membrane potential as a function of the normalized conductance for the different currents recorded from the mitral cells in the saline- and AraC-treated animals. Note that there were no significant differences between different voltage-dependent currents. Data are presented as mean ± SEM ($n = 10$ cells in NaCl and 11 cells in AraC treatment for Na^+ currents; $n = 7$ in both treatments for K^+ currents). ***F***, Confocal images of biocytin-labeled dendrite in NaCl- and AraC-treated OB stained for the postsynaptic GABAergic marker gephyrin. Scale bar, 5 µm. ***G***, Enlarged orthogonal view of the gephyrin puncta indicated by an arrow in ***F***. Scale bar, 2 µm. ***H***, Gephyrin $^+$ punctum density quantification on the mitral cell lateral dendrites for the NaCl- and AraC-treated mice ($n = 9$ cells for control and AraC-treated animals). Each dot represents the value for one single cell. Horizontal bars represent the mean value for all mitral cells for each condition. *$p < 0.05$; Student's t test.

showed a significant reduction in the number of GABAergic synapses of the mitral cells in the AraC-treated mice compared with the control animals (0.147 ± 0.009 and 0.117 ± 0.008 for NaCl- and AraC-treated animals, respectively; $n = 9$ cells in each condition; $p < 0.05$) (Fig. 4*H*). These results indicate that the ablation of neurogenesis reduces the number of GABAergic synapses onto the OB principal neurons, which in turn decreases the inhibitory drive that these neurons receive.

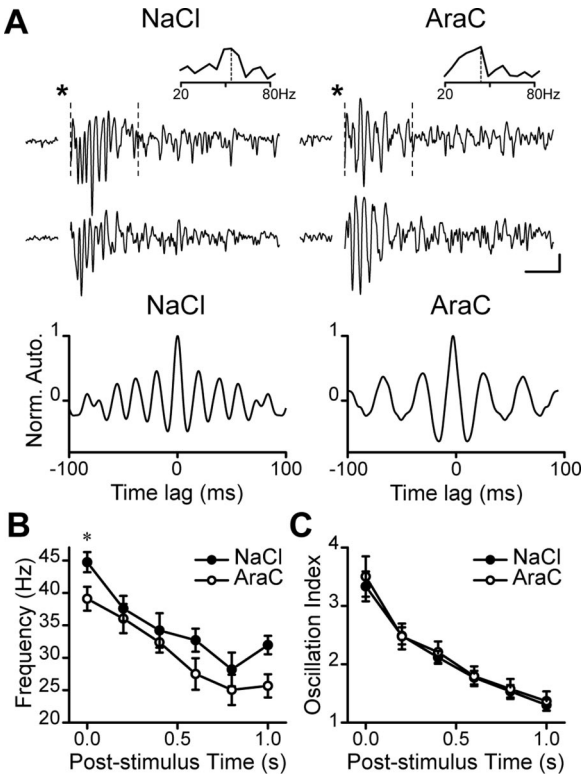

Figure 5. Mice with ablated neurogenesis show reduced network oscillations. ***A***, Top, LFP recordings in slices prepared from NaCl- or AraC-treated animals. Bottom, Autocorrelation graphs computed from traces recorded in the control and AraC-treated OBs. Note the reduced oscillation frequency in AraC-treated mice. Calibration: 50 ms, 20 μV. ***B***, ***C***, Peak frequencies (***B***) and oscillation indexes (***C***) of LFP oscillations in slices derived from control and AraC-treated mice. Data are presented as mean ± SEM ($n = 13$ and 8 slices for control and AraC-treated animals, respectively). *$p < 0.05$; Student's *t* test.

Ablation of neurogenesis reduces the frequency of the induced gamma oscillations in the OB

It is well established that granule-to-mitral cell inhibition plays an important role in generating evoked fast oscillations in the OB (Lagier et al., 2004, 2007). To elucidate whether the changes seen in the OB of the AraC-treated animals would affect the synchronization of the mitral cells we recorded LFPs. The 100 μs stimulation of the olfactory nerve elicited strong LFPs gamma oscillations (20–80 Hz) in the mitral cell layer for both conditions (Fig. 5*A*). As we compared the response properties, we observed a significant reduction in the peak frequency for the slices derived from AraC-treated mice immediately after the stimulation (44.7 ± 1.6 Hz; $n = 13$ slices and 39.1 ± 1.8 Hz; $n = 8$ slices for control and AraC-treated mice, respectively; $p < 0.05$) (Fig. 5*B*). We did not find any significant differences in the peak frequencies measured >200 ms poststimulus interval. The oscillation index, representing the strength of the oscillation, remained unchanged following the ablation of neurogenesis (Fig. 5*C*). These experiments demonstrate that continuous supply of new neurons is required for the maintenance of the synchronized activity of the OB principal cells.

AraC treatment does not impair the general exploratory activity, anxiety, and motivation of animals

Electrophysiological experiments revealed the importance of neurogenesis in the proper bulbar circuitry functioning. It has been suggested that normal inhibitory input on the principal cells is required for an appropriate odor information processing (Saghatelyan et al., 2003) and previous studies have highlighted the link between the level of adult neurogenesis and olfactory performances (Gheusi et al., 2000; Rochefort et al., 2002; Enwere et al., 2004). Surprisingly, however, genetic ablation of adult bulbar neurogenesis did not affect olfactory discrimination and long-term odor-associative memory (Imayoshi et al., 2008). On the basis of these data, we hypothesize that newly generated bulbar interneurons might be involved in some, but not all, odor-associated behavioral tasks. We therefore conducted behavioral studies to elucidate the exact involvement and functional implication of adult bulbar neurogenesis.

Before performing olfactory tests we found it relevant to establish that AraC infusion did not affect the animals' overall locomotor and exploratory activities, motivation and anxiety. We first tested the control and AraC-treated mice in a 60 min locomotion test. The total distances covered by animals of the two groups were very similar ($n = 9$ and $n = 8$ mice for NaCl and AraC groups, respectively) (Fig. 6*A*) suggesting unaltered locomotor activity after AraC infusion. We then tested the mice ability to discriminate the familiarity of previously encountered objects using an object recognition task. This behavioral paradigm is used to assess the directed-motivation and recognition memory of animals (Bevins and Besheer, 2006). After being habituated to the particular object, a new object was presented and the exploration time spent by each mouse was measured. Both control and AraC-infused animals spent longer time exploring a novel object and no significant difference between groups was noticed ($n = 9$ animals for both NaCl- and AraC-treated animals) (Fig. 6*B*). Next, we wanted to exclude any possibility of the anxiety level variations between control and neurogenesis-ablated animals. The similar immobility time during a 6 min tail suspension test demonstrates an unaltered anxiety level for both animal groups ($n = 8$ and n = 7 animals for NaCl- and AraC-treated groups, respectively) (Fig. 6*C*,*D*). Finally, to show that pharmacological ablation of neurogenesis does not affect the spontaneous motivation behavior of animals, we performed a novelty-suppressed feeding behavior test. The feeding latency of food-deprived animals was measured for control and AraC-infused animals and no significant difference between these two groups was observed ($n = 8$ and n = 7 NaCl- and AraC-treated groups, respectively) (Fig. 6*C*,*E*). These control experiments ascertain that pharmacological ablation of adult neurogenesis does not affect locomotor and exploratory behaviors of animals or their anxiety and spontaneous motivation.

Continuous neurogenesis in the OB is required for some but not all odor-associated behavior

We, therefore, examined olfactory performances in mice showing impaired adult OB neurogenesis. We first looked at the odor detection threshold to see whether the ablation of neurogenesis would affect the mouse's odor perception capacity. We submitted the animals to a four-step ascending-concentration series (10^{-7}, 10^{-5}, 10^{-4}, and 10^{-3}) of a given odor (octanol) (Fig. 7*A*) and measured the time that animals spent in investigating the odor versus the mineral oil. A significant increase in the sniffing time of the odor compared with the mineral oil was considered as a characteristic for the animal's odor detection ability. AraC-treated mice were not able to discriminate an odor from mineral oil at concentrations lower than 10^{-3} in comparison with the controls discriminating at 10^{-4} (for octanol: 84.4 ± 5.5% for NaCl, $n = 8$; and 50.9 ± 9.1% for AraC, $n = 9$ mice; *$p < 0.01$) (Fig. 7*A*). In contrast, no differences between groups were observed for the 10^{-3} odor concentrations (80.0 ± 7.3% for NaCl

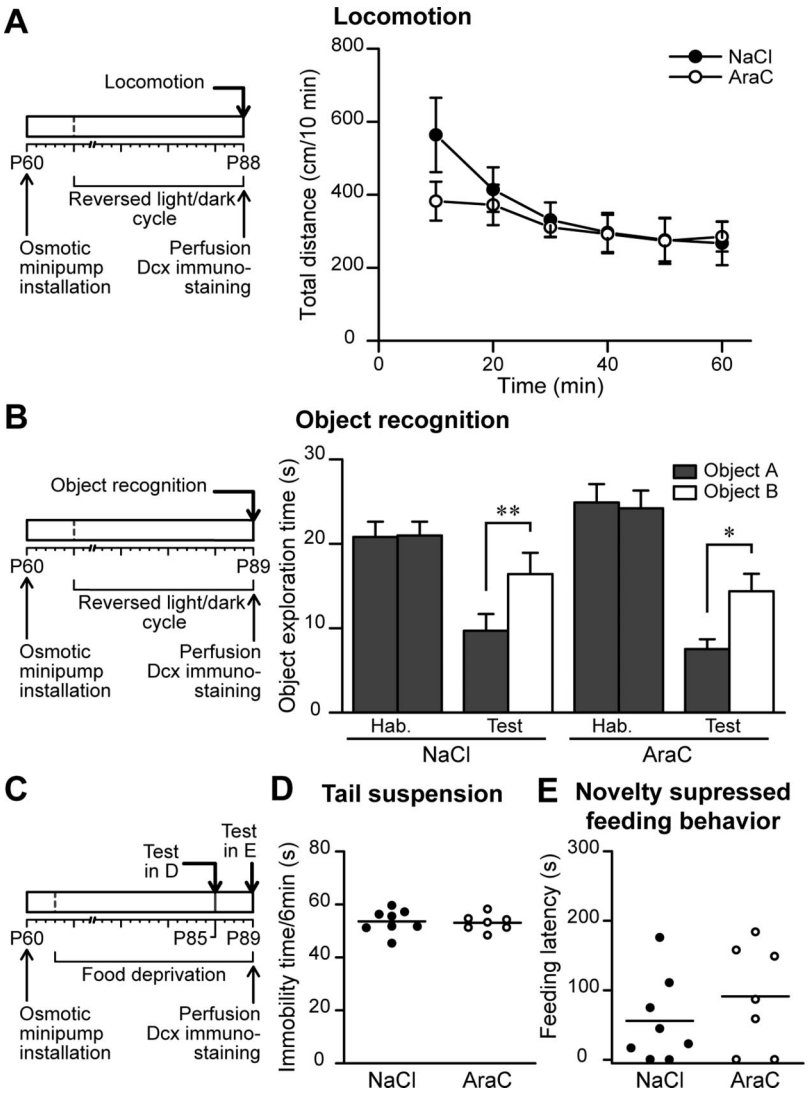

Figure 6. AraC treatment does not affect general locomotor and exploratory activities, anxiety, and motivation of the mouse. ***A***, Left, Experimental design used for the locomotion test. Note that the mice were kept in a reversed light/dark cycle and tested 28 d after pump installation. Right, Results at different time points of the 60 min spontaneous locomotion test. Mice infused with NaCl or with AraC travel the same distance in the locomotion test. Data are presented as mean ± SEM ($n = 9$ and 8 animals for control and AraC-treated group). ***B***, Left, Experimental design used for the object recognition test. The animals were tested 29 d after osmotic minipump installation. Right, Object exploration time in seconds for animals presented with two identical (habituation phase) or two different (test phase) objects. Mice with ablated neurogenesis are able to recognize the object in the same manner as control animals. Data are presented as mean ± SEM ($n = 9$ animals per group). $^*p < 0.05$, $^{**}p < 0.01$; Student's *t* test. ***C***, Experimental design used for the tail suspension test (***D***) and novelty-suppressed feeding behavior test (***E***). Mice used in these test were food deprived. ***D***, Immobility times of NaCl- and AraC-treated mice during a 6 min tail suspension test. Each dot represents the immobility time (in seconds) for one animal. Horizontal bars represent the mean values for all the animals for control and AraC-treated conditions ($n = 8$ and 7 animals, respectively). ***E***, Feeding latencies of mice (in seconds) submitted to a novelty-suppressed feeding behavior test. Each dot represents the feeding latency for one animal, whereas horizontal bars represent the mean value for all the animals from control and AraC-treated conditions ($n = 8$ and 7 animals, respectively).

and 81.1 ± 6.1% for AraC) (Fig. 7*A*). The same results were obtained when isoamyl acetate and limonene-(−) were tested (Fig. 7*A*). Since AraC-infused animals were not different from the control mice in the detection of three different odors at a 10^{-3} concentration, we used this concentration to evaluate odor discrimination (de Chevigny et al., 2006). This test consists of four habituation phases to one odor followed by a dishabituation phase consisting of a novel odor presentation. The exploration time of the novel odor is significantly increased in the presence or not of neurogenesis showing that the constant supply of interneurons to the OB is not required for this task ($n = 9$ and $n = 8$ mice for NaCl- and AraC-treated groups, respectively; $p < 0.01$) (Fig. 7*B*). This result was reproduced with two different pairs of odors (limonene-(−)/2-heptanol and butyraldehyde/isoamyl acetate), although only the limonene-(−)/2-heptanol pair is shown in Figure 7*B*.

We next examined whether a 28 d ablation of neurogenesis would affect long-term odor-associative memory of animals. We used a test based on the ability of the mouse to associate an odor to a reward. This test is based on a previous study using genetic ablation of neurogenesis (Imayoshi et al., 2008). Mice were habituated for 4 d to associate one of two related odors (enantiomers) with a sugar reward placed below bedding. Twenty-four hours and also 7 d after habituation, we tested the mice ability to remember which odor was associated to the rewards by measuring the digging time for each odorant. Both NaCl- and AraC-treated mice spent more time near the odorant previously associated with a sugar reward 1 d or 1 week after habituation ($n = 8$ for both treatments; $^*p < 0.01$ between the two odors) (Fig. 7*C*). These results indicate that acquisition and retention of long-term odor-associated memory does not rely on the continuous supply of new neurons into the bulbar circuitry and are in agreement with recently reported data using animals with genetically ablated bulbar neurogenesis (Imayoshi et al., 2008).

Since the cellular basis for the long-term storage of odor-associative behavior was attributed to the synaptic changes in the piriform cortex (Barkai and Saar, 2001; Quinlan et al., 2004; Roman et al., 2004; Naimark et al., 2007), we also performed a short-term odor memory test shown previously to be dependent of the level of bulbar neurogenesis (Rochefort et al., 2002; Mechawar et al., 2004). This test consisted of two novel odor presentations to the AraC-treated and control mice following defined intervals of 30, 60, 90, and 120 min. The odor concentration use for this test was 10^{-3} as determined in the detection threshold test. The time of sniffing was measured for every odor exposure and it was assumed that an animal remembering an odor will spend less time investigating it on the second presentation (Fig. 7*D*). As expected, the control mice spent a significantly shorter time during the second presentation for all the intervals tested ($n = 8$ animals; $^*p < 0.05$ and $^{**}p < 0.01$) (Fig. 7*D*). In contrast, AraC-treated mice showed only a shorter investigation time on the second presentation at the 30 min interval (first presentation: 8.30 ± 2.08 s; second presentation: 1.70 ± 0.49 s; $^*p < 0.05$) (Fig. 7*D*) and spent equal time investigating an odor during second presentation at the 60, 90, and 120 min intervals ($n = 9$ animals) (Fig. 7*D*). These results

demonstrate that short-term odor memory crucially depends on the continuous neurogenesis in the OB.

Discussion

By suppressing neurogenesis for 25–28 d in the adult mouse OB we demonstrated the role of new neurons in the proper bulbar circuitry functioning. Our electrophysiological analysis at the cellular and network levels revealed, for the first time, the implications of newborn cells in the functional maintenance of OB network. Our behavioral experiments demonstrated that mice with ablated adult neurogenesis showed alterations in some, but not all, odor-associated tasks.

Roles of neurogenesis in the structural and functional maintenance of the OB circuitry

New bulbar interneurons are constantly sent to the OB, where they replace older populations of granule and periglomerular cells (Lagace et al., 2007; Ninkovic et al., 2007; Imayoshi et al., 2008). The importance of adult neurogenesis in this structural maintenance of the bulbar circuitry has been recently revealed by genetic ablation approach when diphtheria toxin (DTA) was conditionally expressed in the Nestin^{+} cells derived progenitors (Imayoshi et al., 2008). Substantial decrease in the overall OB granule cell numbers was demonstrated 6–12 weeks, but not 7–21 d, after the neuronal precursor elimination in adulthood (Imayoshi et al., 2008). Our data showing unaltered number of interneurons in the different granule cell layer regions following pharmacological ablation of neurogenesis for 28 d are consistent with these results. Interestingly, neither genetic (Imayoshi et al., 2008) nor pharmacological (present study) suppressions of bulbar neurogenesis affect the survival rate of pre-existing granule cell populations generated in adulthood. Moreover, the dendritic morphology and spine density of these cells remain unaltered. These data strongly suggest that newly arriving neurons do not provide any instructive and/or supportive roles for the survival and structural complexity of pre-existing granule cells. Continuous flow of new neurons is also not required for the maintenance of mitral cells, the principal neurons in the OB. The lengths of the primary and lateral dendrites, as well as the passive membrane properties of these cells, were not affected by AraC treatment.

In the light of the structural stability of the main neuronal elements (i.e., mitral and pre-existing granule cells) in the OB, it is particularly important to understand how newly generated neurons influence the bulbar network function. To our knowledge, our study provides the first indication of electrophysiological alterations in the OB circuitry following complete ablation of neurogenesis. Our experiments show a decrease in the frequency of the mIPSCs received by the target cells in the condition of suppressed neurogenesis. As a structural mechanism underlying these changes, we identified the reduced number of inhibitory synapses on the mitral cell lateral dendrites. This reduction mostly arises from the arrested arrival of new neurons into the

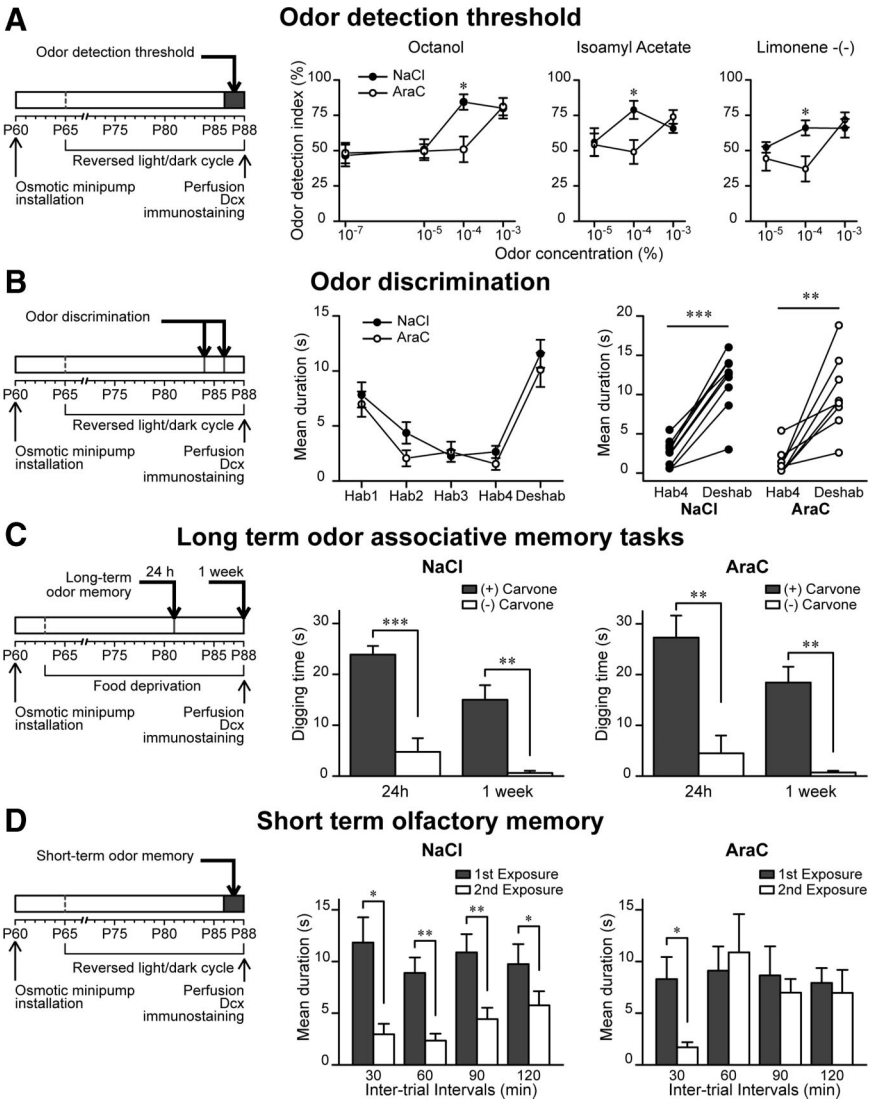

Figure 7. Reduced odor memory in mice with ablated neurogenesis. ***A***, Experimental design (left) and odor detection threshold test in control and AraC-treated mice for three different odors (right). Normalized values are expressed as the mean ratio between the time spent investigating the odor and the total sniffing time (i.e., odor plus mineral oil). Data are presented as mean ± SEM ($n = 8$–9 animals per group). *$p < 0.05$; Student's *t* test. ***B***, Experimental design (left) and odor discrimination test (right) in control (NaCl) and AraC-treated mice. Mice were habituated to an odor with four consecutive presentations. On the fifth presentation a different odor was presented. Both saline-treated and neurogenesis-ablated mice similarly increased the investigation time in response to the new odor. Data are presented as mean ± SEM ($n = 9$ and 8 animals for control and AraC-treated groups). **$p < 0.01$, ***$p < 0.001$ with paired Student's *t* test. ***C***, Left, Experimental design for long-term odor-associative memory tasks. Right, The two groups of animals were trained for 4 d to associate a reward to a carvone-(+) odor. One day and 1 week later, the reward was removed and the digging time was measured when the mouse was exposed to carvone-(+) and carvone-(−). The two graphs represent the digging time 24 h and 1 week after training. Note that in both conditions, mice were able to recognize the reward-associated odor 24 h and 1 week after training. Data are presented as mean ± SEM ($n = 8$ animals per group). **$p < 0.05$, ***$p < 0.01$; Student's *t* test. ***D***, Experimental design (left) and short-term olfactory memory test (right) in control (NaCl) and AraC-treated mice. Each bar represents the mean time spent investigating a given odor on the first (gray columns) and second (white columns) odor exposures. Note that control animals remember the first exposure of the odor 30, 60, 90, and 120 min later, whereas AraC-treated mice remember only 30 min later. Data are presented as mean ± SEM ($n = 8$ animals for NaCl- and $n = 9$ for AraC-treated mice). *$p < 0.05$, **$p < 0.01$ with paired Student's *t* test.

OB since the spine density of pre-existing granule cells was not changed. Interestingly, while the frequency of mIPSCs was reduced by ~45%, only 20% of reduction in gephryn$^+$ puncta on the lateral dendrites of mitral cells was observed. It should be noted, however, that because of the sensitivity of our immunohistochemical analysis of GABAergic synapses we might have underestimated the real proportion of reduction. Indeed, previous electron microscopy studies demonstrated a 46% reduction in granule-to-mitral cell synapses following 30 d of sensory deprivation (Benson et al., 1984). Alternatively, it is conceivable that newborn neurons, compared with the pre-existing granule cells, contribute to a much larger degree to the overall inhibitory input received by the principal neurons. Indeed, electrophysiological recordings and analysis of immediate early gene expression pattern following modulation of sensory input have revealed contrasting responses of granule cells born during early postnatal period and in adulthood (Magavi et al., 2005; Saghatelyan et al., 2005). In addition, it has been recently shown that excitatory synapses received by newborn granule cells shortly after their arrival into the OB undergo long-term potentiation which, in turn, might increase inhibition from these cells onto principal neurons (Nissant et al., 2009). This plasticity was not observed at the synapses made onto the pre-existing granule cells or newborn neurons at the later stages of their maturation (Nissant et al., 2009). Altogether, these data suggest that the level of inhibition provided by granule cells onto the dendrite of principal neurons depends on the maturational stage of these interneurons. While this hypothesis requires further confirmation, it is also compatible with previous report showing a similar decrease in the mIPSCs frequency when an abnormal newly born granule cell spine density was detected in the sensory-deprived animals (Saghatelyan et al., 2005).

Importantly, the amplitudes of spontaneous inhibitory events as well as their kinetics were not modified by AraC treatment, indicating for the normal content and functioning of postsynaptic $GABA_A$ receptors. Moreover, by calculating the percentage of reduction in the frequency and amplitude of spontaneous events following the blockade of glutamatergic transmission and action potential we demonstrated unaltered glutamate-induced and action potential-mediated GABA release. Thus, ablated neurogenesis give rises to an overall reduced number of inhibitory synapses on the OB principal cells that, in turn, underlie reduction in the mIPSCs frequency. The decreased frequency of miniatures has an important functional consequence on the entire bulbar network since both evoked and total spontaneous inhibitory activity (including action potential and glutamate-induced GABA release components) were also reduced.

It is well established that granule cells are involved in the synchronization of the OB relay neurons: the mitral cells (Lagier et al., 2004). Altered inhibitory synaptic inputs to these principal neurons seen in AraC-treated animals resulted in a decreased synchronized oscillatory activity in the mitral cell layer. Previous computational and electrophysiological studies in the hippocampus and the cortex revealed that the frequency of gamma oscillations largely depends on the kinetics and amplitude of inhibitory currents (Wang and Buzsáki, 1996; Whittington et al., 2000; Traub et al., 2004). Interestingly, while kinetics and amplitude of unitary miniature IPSCs recorded from the mitral cells in the neurogenesis-deficient OB were not affected, the amplitude of the dendrodendritic recurrent inhibition was drastically reduced. The reduction in the amplitude of dendrodendritic recurrent inhibition (and likely lateral inhibition) results from the decreased number of inhibitory synapses observed in the AraC-treated animals. These data are in line with findings showing reduced amplitude of dendrodendritic inhibitory current in mice with affected number of functional synapses (Lagier et al., 2007). This, in turn, results in the reduced frequency of gamma oscillations in the OB network (Lagier et al., 2007). Importantly, modeling studies showed that network oscillation frequencies in the OB would be sensitive to the inhibitory event occurrence probability (Lagier et al., 2007). Indeed, a decrease in the miniature IPSCs frequency was observed in animals showing reduced frequency of gamma oscillations (Lagier et al., 2007). These data are in line with our findings and support the notion that the reduction in the frequency of the induced gamma oscillations in the OB is directly linked to the decrease in the number of inhibitory synapses on the mitral cells. The synchronized activity of OB principal cells is believed to be supported either by the lateral and recurrent inhibition (Schoppa and Urban, 2003; Lledo and Lagier, 2006) or by correlated but aperiodic inputs received from common granule cells (Galán et al., 2006). While the first hypothesis stipulates that recurrent and lateral inhibition mediated by dendrodendritic reciprocal synapses allows simultaneous resumption of firing activity of population of mitral cells, the second model states that OB principal neurons are firing in a roughly oscillatory pattern and that their activity is synchronized by the common input from granule cell. Importantly, our data showing complete loss of newly generated neurons following AraC treatment as well as reduction in the overall number of inhibitory synapses are compatible with both models. Altogether, our results show for the first time the physiological changes in the OB circuitry at the cellular and network levels following ablation of neurogenesis.

Newborn neurons are involved in the execution of selected olfactory behaviors

Mitral cell synchronization is thought to be implicated in the odor information processing (Laurent et al., 2001; Saghatelyan et al., 2003; Lledo and Lagier, 2006). Olfactory discrimination learning tasks increase the survival of newly born cells in the OB (Alonso et al., 2006; Mandairon et al., 2006). This implies that neurogenesis is important for the maintenance of normal olfactory behavior. Indeed, a clear correlation was established when mice exposed to an enriched environment displayed both an increased neurogenesis and short-term olfactory memory (Rochefort et al., 2002). In addition, animals showing reduced neurogenesis also display alterations in fine olfactory discrimination (Enwere et al., 2004). However, it has been recently reported that genetic ablation of bulbar neurogenesis is not associated with a noticeable defect in odor discrimination and long-term olfactory memory (Imayoshi et al., 2008). Our data showing unaltered olfactory discrimination following pharmacological ablation of new bulbar neurons support these observations. It is noteworthy that in our study as well as in that of Imayoshi and colleagues (Imayoshi et al., 2008), odor discrimination between two discrete odors was assessed. It has been previously shown that mice with reduced level of bulbar neurogenesis perform normally in the discrimination task between two discrete odors (Enwere et al., 2004); but see also (Gheusi et al., 2000) but have alterations in the fine olfactory discrimination between similar odors (Enwere et al., 2004). Thus, it is conceivable that newborn bulbar interneurons might be exclusively involved in the olfactory discrimination fine tuning when animals needs to identify and extract tiny traces of novel odor from the complex odorant environment.

Newborn neurons also do not participate in the acquisition and retention of long-term odor memory. The animals with both genetic (Imayoshi et al., 2008) and pharmacological (present study) ablations of adult bulbar neurogenesis perform normally

in the odor memory task. This particular memory task is based on the discrimination of the discrete odors that are associated with reward. It has been shown that association of sensory stimuli with reward occurs in the cortical areas (Ressler, 2004; Kelley et al., 2005; Phillmore, 2008; Rolls and Grabenhorst, 2008). Indeed, odor-associated learning induces substantial changes in the piriform cortex, where augmented expression of neurotrophic factors, increased neuronal excitability, and enlarged synaptic transmission and plasticity are observed (Barkai and Saar, 2001; Quinlan et al., 2004; Naimark et al., 2007). Since newborn neurons are not involved in the discrimination of the discrete odors (Enwere et al., 2004) (present study) and the cellular basis for odor-associated learning seems to operate in the piriform cortex (Barkai and Saar, 2001; Quinlan et al., 2004; Naimark et al., 2007), it is therefore expected that animals with ablated neurogenesis perform normally in this particular memory task. To reveal the role of adult neurogenesis in the olfactory memory we, thus, used a spontaneous short-term memory paradigm that has been shown to be correlated with the level of newborn neurons in the OB (Rochefort et al., 2002). Our results demonstrate that ablating bulbar neurogenesis during a period of 25–28 d gives rise to significant alterations in the short-term odor memory. It is unlikely that the differences observed in the short-term memory task are mediated by the reduced neurogenesis in the dentate gyrus. It has been recently demonstrated that ablation of neurogenesis in the dentate gyrus that lead to the affected contextual and spatial memories does not alter animal performances in the odor discrimination and memory tasks (Imayoshi et al., 2008). In addition, we used similar experimental design in terms of spatial and contextual characteristics for short-term memory, olfactory discrimination, and odor-associated long-term memory paradigms and observed alterations exclusively in the spontaneous short-term memory task. These results suggest that newborn neurons are involved in the execution of specific odor-associated behavioral tasks. Finally, we also see subtle changes in the odor detection in AraC-treated animals, which can be related to the reduction in the number of periglomerular cells as previously suggested (Wachowiak and Shipley, 2006).

Altogether, our data provide first evidence for the functional involvement of newly born neurons in the OB cellular network and show that these changes affect some, but not all, olfactory behaviors.

References

Alonso M, Viollet C, Gabellec MM, Meas-Yedid V, Olivo-Marin JC, Lledo PM (2006) Olfactory discrimination learning increases the survival of adult-born neurons in the olfactory bulb. J Neurosci 26:10508–10513.

Barkai E, Saar D (2001) Cellular correlates of olfactory learning in the rat piriform cortex. Rev Neurosci 12:111–120.

Belluzzi O, Benedusi M, Ackman J, LoTurco JJ (2003) Electrophysiological differentiation of new neurons in the olfactory bulb. J Neurosci 23:10411–10418.

Benson TE, Ryugo DK, Hinds JW (1984) Effects of sensory deprivation on the developing mouse olfactory system: a light and electron microscopic, morphometric analysis. J Neurosci 4:638–653.

Bevins RA, Besheer J (2006) Object recognition in rats and mice: a one-trial non-matching-to-sample learning task to study 'recognition memory.' Nat Protoc 1:1306–1311.

Britton DR, Britton KT (1981) A sensitive open field measure of anxiolytic drug activity. Pharmacol Biochem Behav 15:577–582.

Carlén M, Cassidy RM, Brismar H, Smith GA, Enquist LW, Frisén J (2002) Functional integration of adult-born neurons. Curr Biol 12:606–608.

Carleton A, Petreanu LT, Lansford R, Alvarez-Buylla A, Lledo PM (2003) Becoming a new neuron in the adult olfactory bulb. Nat Neurosci 6:507–518.

Crowley JJ, Jones MD, O'Leary OF, Lucki I (2004) Automated tests for measuring the effects of antidepressants in mice. Pharmacol Biochem Behav 78:269–274.

de Chevigny A, Lemasson M, Saghatelyan A, Sibbe M, Schachner M, Lledo PM (2006) Delayed onset of odor detection in neonatal mice lacking tenascin-C. Mol Cell Neurosci 32:174–186.

Enwere E, Shingo T, Gregg C, Fujikawa H, Ohta S, Weiss S (2004) Aging results in reduced epidermal growth factor receptor signaling, diminished olfactory neurogenesis, and deficits in fine olfactory discrimination. J Neurosci 24:8354–8365.

Galán RF, Fourcaud-Trocmé N, Ermentrout GB, Urban NN (2006) Correlation-induced synchronization of oscillations in olfactory bulb neurons. J Neurosci 26:3646–3655.

Gheusi G, Cremer H, McLean H, Chazal G, Vincent JD, Lledo PM (2000) Importance of newly generated neurons in the adult olfactory bulb for odor discrimination. Proc Natl Acad Sci U S A 97:1823–1828.

Hack MA, Saghatelyan A, de Chevigny A, Pfeifer A, Ashery-Padan R, Lledo PM, Götz M (2005) Neuronal fate determinants of adult olfactory bulb neurogenesis. Nat Neurosci 8:865–872.

Imayoshi I, Sakamoto M, Ohtsuka T, Takao K, Miyakawa T, Yamaguchi M, Mori K, Ikeda T, Itohara S, Kageyama R (2008) Roles of continuous neurogenesis in the structural and functional integrity of the adult forebrain. Nat Neurosci 11:1153–1161.

Kelley AE, Schiltz CA, Landry CF (2005) Neural systems recruited by drug- and food-related cues: studies of gene activation in corticolimbic regions. Physiol Behav 86:11–14.

Lagace DC, Whitman MC, Noonan MA, Ables JL, DeCarolis NA, Arguello AA, Donovan MH, Fischer SJ, Farnbauch LA, Beech RD, DiLeone RJ, Greer CA, Mandyam CD, Eisch AJ (2007) Dynamic contribution of nestin-expressing stem cells to adult neurogenesis. J Neurosci 27:12623–12629.

Lagier S, Carleton A, Lledo PM (2004) Interplay between local GABAergic interneurons and relay neurons generates gamma oscillations in the rat olfactory bulb. J Neurosci 24:4382–4392.

Lagier S, Panzanelli P, Russo RE, Nissant A, Bathellier B, Sassoè-Pognetto M, Fritschy JM, Lledo PM (2007) GABAergic inhibition at dendrodendritic synapses tunes gamma oscillations in the olfactory bulb. Proc Natl Acad Sci U S A 104:7259–7264.

Laurent G, Stopfer M, Friedrich RW, Rabinovich MI, Volkovskii A, Abarbanel HD (2001) Odor encoding as an active, dynamical process: experiments, computation, and theory. Annu Rev Neurosci 24:263–297.

Lemasson M, Saghatelyan A, Olivo-Marin JC, Lledo PM (2005) Neonatal and adult neurogenesis provide two distinct populations of newborn neurons to the mouse olfactory bulb. J Neurosci 25:6816–6825.

Lledo PM, Lagier S (2006) Adjusting neurophysiological computations in the adult olfactory bulb. Semin Cell Dev Biol 17:443–453.

Lledo PM, Saghatelyan A (2005) Integrating new neurons into the adult olfactory bulb: joining the network, life-death decisions, and the effects of sensory experience. Trends Neurosci 28:248–254.

Magavi SS, Mitchell BD, Szentirmai O, Carter BS, Macklis JD (2005) Adult-born and preexisting olfactory granule neurons undergo distinct experience-dependent modifications of their olfactory responses in vivo. J Neurosci 25:10729–10739.

Mak GK, Enwere EK, Gregg C, Pakarainen T, Poutanen M, Huhtaniemi I, Weiss S (2007) Male pheromone-stimulated neurogenesis in the adult female brain: possible role in mating behavior. Nat Neurosci 10:1003–1011.

Mandairon N, Sacquet J, Garcia S, Ravel N, Jourdan F, Didier A (2006) Neurogenic correlates of an olfactory discrimination task in the adult olfactory bulb. Eur J Neurosci 24:3578–3588.

Mechawar N, Saghatelyan A, Grailhe R, Scoriels L, Gheusi G, Gabellec MM, Lledo PM, Changeux JP (2004) Nicotinic receptors regulate the survival of newborn neurons in the adult olfactory bulb. Proc Natl Acad Sci U S A 101:9822–9826.

Naimark A, Barkai E, Matar MA, Kaplan Z, Kozlovsky N, Cohen H (2007) Upregulation of neurotrophic factors selectively in frontal cortex in response to olfactory discrimination learning. Neural Plast 2007:13427.

Ninkovic J, Mori T, Götz M (2007) Distinct modes of neuron addition in adult mouse neurogenesis. J Neurosci 27:10906–10911.

Nissant A, Bardy C, Katagiri H, Murray K, Lledo PM (2009) Adult neurogenesis promotes synaptic plasticity in the olfactory bulb. Nat Neurosci 12:728–730.

Phillmore LS (2008) Discrimination: from behaviour to brain. Behav Processes 77:285–297.

Price JL, Powell TP (1970) The synaptology of the granule cells of the olfactory bulb. J Cell Sci 7:125–155.

Quinlan EM, Lebel D, Brosh I, Barkai E (2004) A molecular mechanism for stabilization of learning-induced synaptic modifications. Neuron 41:185–192.

Ressler N (2004) Rewards and punishments, goal-directed behavior and consciousness. Neurosci Biobehav Rev 28:27–39.

Rochefort C, Gheusi G, Vincent JD, Lledo PM (2002) Enriched odor exposure increases the number of newborn neurons in the adult olfactory bulb and improves odor memory. J Neurosci 22:2679–2689.

Rolls ET, Grabenhorst F (2008) The orbitofrontal cortex and beyond: from affect to decision-making. Prog Neurobiol 86:216–244.

Roman FS, Truchet B, Chaillan FA, Marchetti E, Soumireu-Mourat B (2004) Olfactory associative discrimination: a model for studying modifications of synaptic efficacy in neuronal networks supporting long-term memory. Rev Neurosci 15:1–17.

Saghatelyan A, Carleton A, Lagier S, de Chevigny A, Lledo PM (2003) Local neurons play key roles in the mammalian olfactory bulb. J Physiol Paris 97:517–528.

Saghatelyan A, Roux P, Migliore M, Rochefort C, Desmaisons D, Charneau P, Shepherd GM, Lledo PM (2005) Activity-dependent adjustments of the inhibitory network in the olfactory bulb following early postnatal deprivation. Neuron 46:103–116.

Schoppa NE, Urban NN (2003) Dendritic processing within olfactory bulb circuits. Trends Neurosci 26:501–506.

Shingo T, Gregg C, Enwere E, Fujikawa H, Hassam R, Geary C, Cross JC, Weiss S (2003) Pregnancy-stimulated neurogenesis in the adult female forebrain mediated by prolactin. Science 299:117–120.

Snapyan M, Lemasson M, Brill MS, Blais M, Massouh M, Ninkovic J, Gravel C, Berthod F, Götz M, Barker PA, Parent A, Saghatelyan A (2009) Vasculature guides migrating neuronal precursors in the adult mammalian forebrain via brain-derived neurotrophic factor signaling. J Neurosci 29:4172–4188.

Traub RD, Bibbig A, LeBeau FE, Buhl EH, Whittington MA (2004) Cellular mechanisms of neuronal population oscillations in the hippocampus in vitro. Annu Rev Neurosci 27:247–278.

Wachowiak M, Shipley MT (2006) Coding and synaptic processing of sensory information in the glomerular layer of the olfactory bulb. Semin Cell Dev Biol 17:411–423.

Wang XJ, Buzsáki G (1996) Gamma oscillation by synaptic inhibition in a hippocampal interneuronal network model. J Neurosci 16:6402–6413.

Whitman MC, Greer CA (2007) Synaptic integration of adult-generated olfactory bulb granule cells: basal axodendritic centrifugal input precedes apical dendrodendritic local circuits. J Neurosci 27:9951–9961.

Whittington MA, Traub RD, Kopell N, Ermentrout B, Buhl EH (2000) Inhibition-based rhythms: experimental and mathematical observations on network dynamics. Int J Psychophysiol 38:315–336.